ICAST2014 #056

Design studies on cellular structures with pneumatic artificial muscle inclusions for modulus variation

Michael E. Pontecorvo, Robert J. Niemiec, Farhan S. Gandhi *

Rensselaer Polytechnic Institute, Troy, NY 12180, USA

Abstract

This paper presents a novel variable modulus cellular structure based on a hexagonal unit cell with pneumatic artificial muscle (PAM) inclusions. The cell considered is pin-jointed, loaded in the horizontal direction, with three PAMs (one vertical PAM and two horizontal PAMs) oriented in an "H" configuration between the vertices of the cell. A method for calculation of the hexagonal cell modulus is introduced, as is an expression for the balance of tensile forces between the horizontal and vertical PAMs. An aluminum hexagonal unit cell is fabricated and simulation of the hexagonal cell with PAM inclusions is then compared to experimental measurement of the unit cell modulus in the horizontal direction over a pressure range up to 682 kPa. An increase in cell modulus of 200% is demonstrated experimentally, with a minimum change in cell geometry. A design study via simulation predicts that differential pressurization of the PAMs up to 1992 kPa can increase the cell modulus in the horizontal direction by a factor of 6.66. A design study considering parametric variation in cell angle, vertical to inclined wall length ratio, and PAM contraction ratios showed that changes in modulus of over 1000% were possible by differential pressurization of the PAMs. Both experiment and simulation show that this concept provides a way to decouple the length change of a PAM from the change in modulus to create a structural unit cell whose in-plane modulus in a given direction can be tuned based on the orientation of PAMs within the cell and the pressure supplied to the individual muscles.

1. INTRODUCTION

A recent study by Pontecorvo et al.[1] proposed a framework in which rigid-link, pin-jointed hexagonal unit cells can be supported internally by a variety of passive inclusions – such as springs[1], buckling beams[2], or dampers[2,3] – in order to tailor the in-plane behavior of the cells to specific functions. It was found that three inclusions between the vertices were necessary for the cell to be statically determinate. In the case of linear spring inclusions, expressions for the modulus of the cell in the vertical and horizontal directions were derived based on the stiffness of the springs[1].

This work builds on the concept proposed by Pontecorvo et al. by including pneumatic artificial muscles (PAMs) as semi-active, variable stiffness springs within the unit cell. PAMs were first patented by Gaylord[4] in 1958 and used by McKibben as orthotic devices in the 1950s[5]. Each PAM consists of a cylindrical flexible rubber bladder surrounded by a braided mesh of fibers that are connected to end

* Corresponding author, E-mail: fgandhi@rpi.edu

fittings. When the bladder is inflated with pressure from a fluid (usually air), the radial expansion tensions the braided fibers and causes the muscle to contract axially. A characteristic of PAMs is that the stiffness of the actuator is directly proportional to pressure. Several researchers have explored using this property to vary the stiffness or elastic modulus of structures. Philen[6-10], for example, has demonstrated experimentally that flexible fluidic matrix composite (F^2MC) tubes can change modulus by a factor of 50. F^2MCs are similar to PAMs but with fibers embedded in the bladder (in place of the external braided mesh) to form a composite cylinder. They are typically filled with high bulk modulus fluid rather than air. Philen[8] and Chen et al.[11] have investigated using F^2MC tubes embedded within an elastomeric matrix to create variable stiffness panels. Kim et al.[12] applied the F^2MC in a similar way to create a variable bending stiffness composite beam.

The current study presents a novel variable modulus structural element by incorporating PAMs within a hexagonal unit cell. Using an orthogonal arrangement of PAMs provides a way to largely decouple the length change of a PAM from the change in modulus to create a structural unit cell whose in-plane modulus in a given direction can be tuned based on the orientation of PAMs within the cell and the pressure supplied to the individual muscles. These unit cells can then be repeated in-plane or stacked in layers to create a composite structure whose modulus and load-deformation coupling can be actively tuned using fluid pressure. The paper describes the fabrication of a pin-jointed hexagonal unit cell with two horizontal PAMs and one vertical PAM arranged in an "H" configuration, as seen in Figure 1. The cell is loaded in the horizontal (x) direction and its modulus (E_x) is measured for increasing values of pressure in the PAMs. The measurements are compared to simulation results and the model is further used to predict the largest changes in modulus that could be achieved through differential pressurization of the horizontal and vertical PAMs. The paper provides an understanding of the mechanisms by which cell modulus change is achieved, and also presents a design study examining achievable modulus change in various cell geometries.

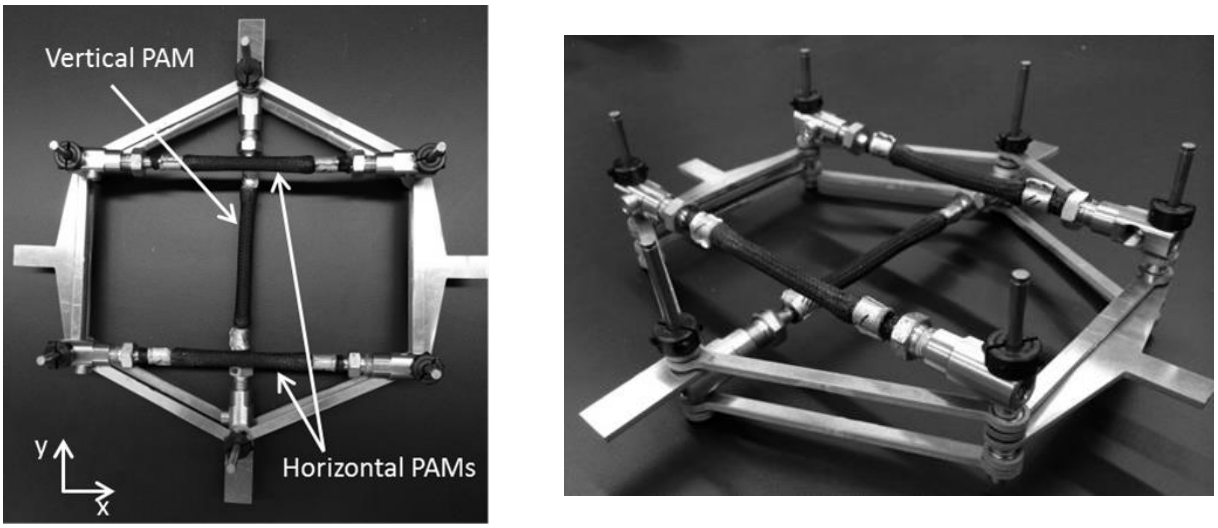

(a) (b)

Figure 1. (a) Top view and (b) isometric view of the prototype hexagonal cell with one vertical PAM and two horizontal PAMs

2. ANALYSIS

2.1 PAM model

The constitutive behavior of an individual PAM was modeled based on the modeling approach for PAMs developed by Kothera et al.[13] A schematic on which their model is based is shown in Figure 2. The PAM comprises a tubular elastomeric bladder of active length L, outer radius R, wall thickness t, and elastic modulus E, over which a single fiber of length b is wrapped N times at an angle θ_b. Kothera et al. assume that the volume of the bladder material, V_b, does not change from its original volume, V_{b0}, as described in Equation 1, and use this relationship to find the bladder wall thickness t at any muscle length L. When pressurized to a pressure P, stresses in the bladder develop in the circumferential direction, σ_c, and in the axial direction, σ_z. The corresponding axial force in the bladder and tension, T, in the fiber are in equilibrium with the applied axial force, F, at the free end of the PAM. The result is Equation 2, which relates the applied axial force to the length of the PAM for a given pressure. This equation is used throughout the current work to simulate the force-displacement behavior of the individual PAMs and is integrated into the hexagonal unit cell to calculate its modulus. A non-cylindrical tip-shape correction was not applied to Equation 2 because it was not found to improve the correlation of the simulation with experiment, nor was friction included in the model.

$$V_b = L(\pi R^2 - \pi(R-t)^2) = V_{b0} = L_0\left(\pi {R_0}^2 - \pi(R_0 - t_0)^2\right) \quad (1)$$

$$F = \frac{P\left(3L^2 - b^2\right)}{4N^2\pi} + EV_b\left(\frac{1}{L_0} - \frac{1}{L}\right) + P\left(\frac{V_b}{L} - \frac{tL^2}{2\pi RN^2}\right) + \frac{EL}{2\pi RN^2}(tL - t_0L_0) \quad (2)$$

Before introducing the PAMs into the hexagonal cells, tensile load versus contraction ratio ($\mathrm{CR} = L/L_0$) measurements for individual PAMs were obtained and compared to simulation results based on Equation 2. For the simulation, the two muscle parameters that were measured most precisely – the muscle active length and bladder wall thickness – were directly used as input parameters. Starting with initial estimates, the muscle braid length, b, initial radius, R_0, and bladder elastic modulus, E, were adjusted to best match the experimental results. The values of bladder elastic modulus and initial radius were taken to be the same for both the horizontal muscles and the vertical muscle (since they were fabricated from the same tube). The final values chosen for the simulation are listed with the measured values in Table 1. Owing to the geometry of a regular hexagonal cell, the horizontal PAMs' initial active length, L_0, and braid length, b, are shorter than those of the vertical PAM. The values of b used in the simulation correspond to a braid angle of 53.58° for the vertical PAM and 52.39° for the horizontal PAMs.

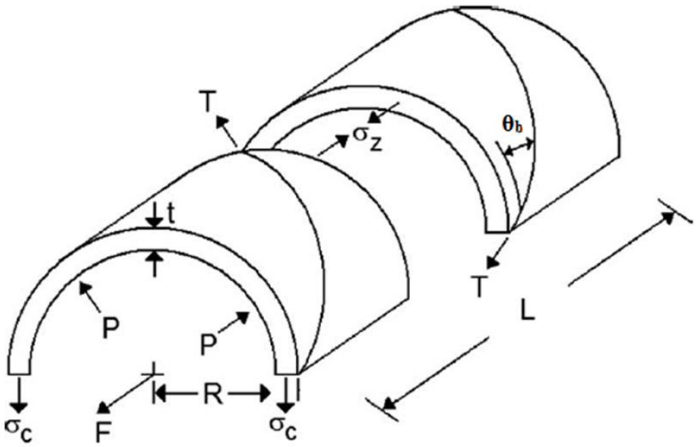

Figure 2. Schematic of Kothera et al.'s PAM force-balance model[13]

Table 1. PAM parameters

Parameter	Vertical PAM		Horizontal PAMs	
	Measured	Simulation	Measured	Simulation
L_0 (m)	0.0909	0.0909	0.0507	0.0507
b (m)	-	0.1130	-	0.0640
t_0 (m)	0.0008	0.0008	0.0008	0.0008
R_0 (m)	0.0043	0.0048	0.0043	0.0048
E (MPa)	-	3	-	3

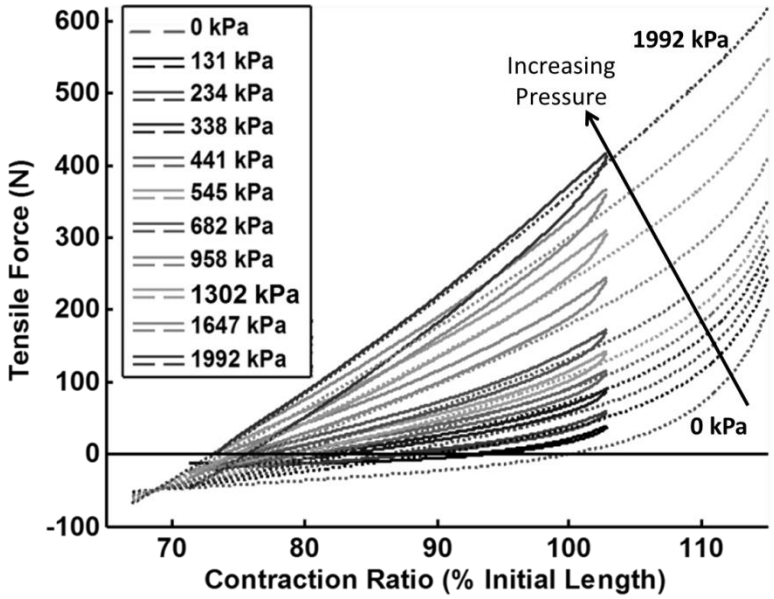

Figure 3. Tensile force versus contraction ratio over a range of pressures for the vertical PAM. Dotted lines represent simulation, solid lines represent measured data.

Figure 3 is a plot of the tensile force as a function of contraction ratio for the vertical PAM over a range of pressures up to 1992 kPa. The solid lines represent measured experimental data obtained from tests conducted in an Instron 4204 machine, and the dotted lines represent the simulation results based on the parameters listed in Table 1. The vertical muscle was tested at pressures from 131 to 1992 kPa up to a contraction ratio of 103%. The simulation is plotted at the same pressures as the experiment with an additional curve at 0 kPa, and up to a contraction ratio of 115%. At pressures below 441 kPa, the simulation slightly overpredicts the tensile force of the actuator vis-à-vis the experimental results. Above 441 kPa the simulations slightly underpredict the experimental curves until the final pressure of 1992 kPa. This spread of the simulation results are sensitive to the chosen simulation parameters and the results presented in Figure 3 reflect the best fit of the simulation to the experiment over the range of pressures. For clarity, Figure 4 shows a comparison of the vertical PAM experimental and simulation results at a single pressure of 682 kPa. Overall, the slope of the simulated curve compares well with the experiment, but the predicted free length (corresponding to zero tensile force) is slightly higher than the experiment, and the simulation shows less nonlinearity (stiffening behavior) at higher contraction ratios. In the current study the PAMs never enter compression when arranged in the hexagonal cell for the range of pressures and displacements investigated.

Results similar to those seen in Figure 3 are presented in Figure 5 for the horizontal PAMs. The experimental data (solid curves) represents the average of the two horizontal PAMs while the simulation results are presented by the dashed curves. The PAM blocked force and free length for increasing pressures (obtained from Figure 3 and 5) are summarized in Figure 6a and 6b, respectively. In Figure 6a,

the blocked force of the vertical PAM is larger than the blocked force of the horizontal PAMs in both simulation (by 11.4% at 1992 kPa) and experiment (by 9.9% at 1992 kPa). Likewise, in Figure 6b, the free length of the vertical PAM is always lower than the free length of the horizontal PAMs. If the initial braid angle, θ_{b0}, of the PAMs were equal, the simulation curves of the vertical and horizontal PAMs would lie on top of each other. The difference then corresponds to the difference in initial braid angle (53.58^o for the vertical muscle, and 52.39^o for the horizontal PAMs), which increases the blocked force and decreases the free length for the vertical PAM over the horizontal PAMs. The braid angle of the prototype PAMs is difficult to measure accurately, but the fact that this same trend is present in the experimental results indicates that the initial braid angle of the vertical PAM as fabricated is likely about a degree higher than the initial braid angle of the horizontal PAMs.

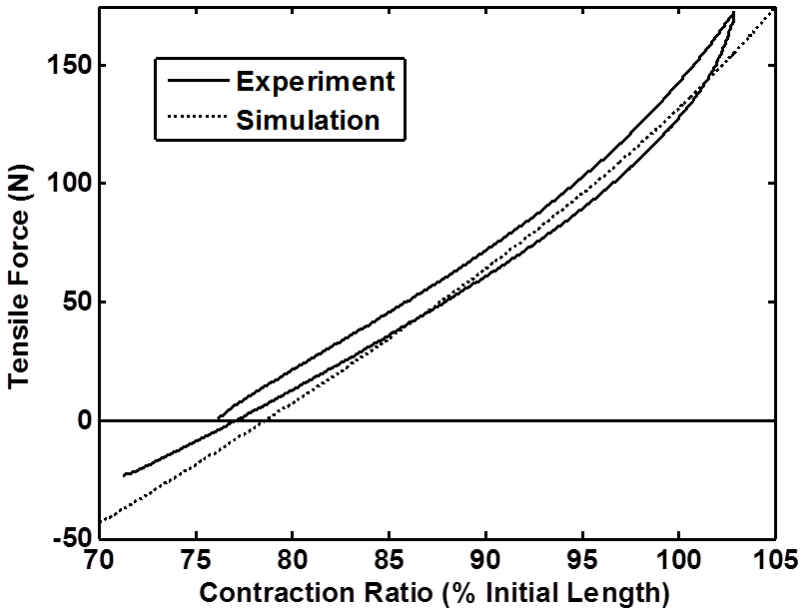

Figure 4. Tensile force versus contraction ratio for the vertical PAM at 682 kPa.

2.2 Hexagonal unit cell analysis and modulus calculation

The pin-jointed hexagonal unit cell used in this study is based on the cell presented in Pontecorvo et al.[1], a schematic of which is shown in Figure 7. The cell walls were rigid links and the pin-joints at the cell vertices highlighted the effects of the internal inclusions as these were not masked by the influence of cell wall bending. The basic unit cell is composed of inclined walls of length L_{link} that form an angle θ with the horizontal, vertical walls of length αL_{link}, and includes half the vertical wall, $\alpha L_{link}/2$, of the adjacent cells above and below the cell. The depth of the cell (into the page) is denoted as γL_{link}. Pontecorvo et al. showed that three spring elements connected between the vertices of the cell were necessary in order for the cell to be statically determinate and derived expressions for the modulus of the cell under both horizontal and vertical loading based on the stiffness of the three springs when arranged in the configuration shown in Figure 7. It was also demonstrated that the total modulus of the cell is given by the sum of the modulus due to the horizontal spring and the modulus due to the vertical spring.

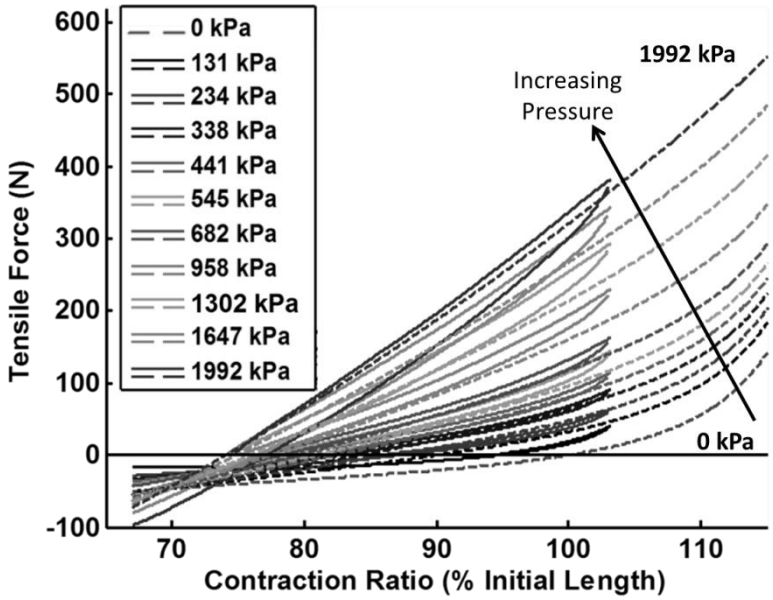

Figure 5. Averaged tensile force versus contraction ratio over a range of pressures for the horizontal PAMs. Dashed lines represent simulation, solid lines represent measured data.

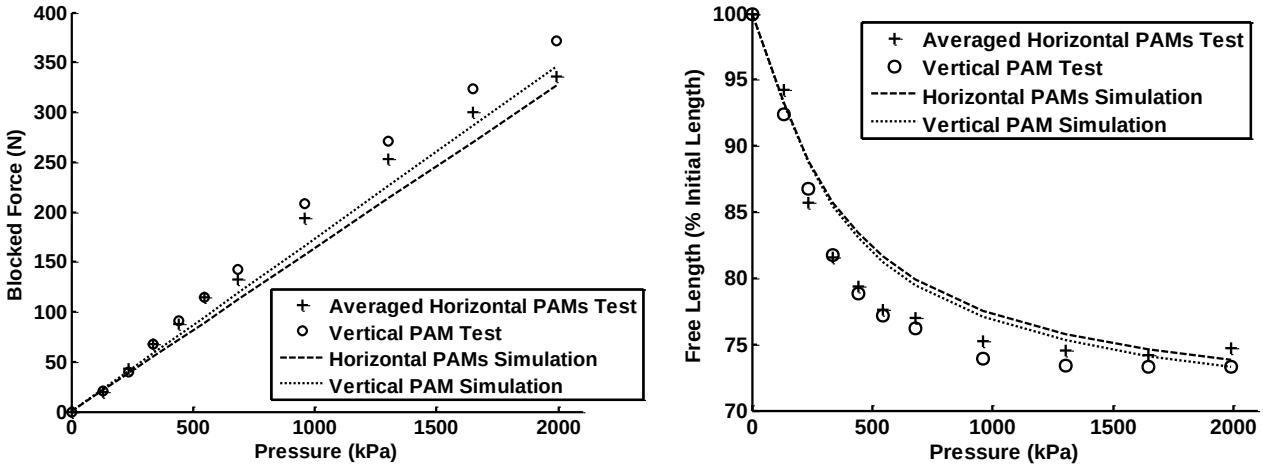

(a) (b)

Figure 6. Comparison of experimental and simulated (a) blocked force and (b) free length of the individual muscles.

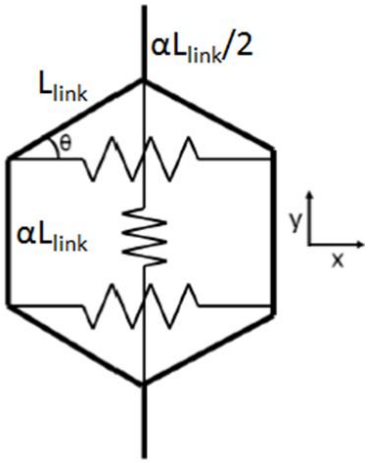

Figure 7. A pin-jointed hexagonal unit cell with three linear spring inclusions (two horizontal and one vertical) oriented in an "H" pattern between the vertices of the cell.[1]

The current study takes a similar approach to the calculation of the cell modulus, where the linear springs of the previous work are replaced by PAMs whose nonlinear behavior is represented by Equation 2. Since the PAMs carry load in tension, they are sufficiently pre-tensioned such that even as the cell is subjected to tensile and compressive loading, the individual PAMs only operate in tension.

To account for the introduction of the PAMs into the unit cell, consider the schematics of the unit cells loaded by an applied stress in the horizontal (x) direction depicted in Figure 8. The expressions for the stress applied in the horizontal direction, σ_x, and the strain in the horizontal direction, ε_x, are given by Equations 3 and 4, respectively. In Figure 8a where the two PAMs in the cell are oriented horizontally, $F_X = 2F_H$, and similarly for Figure 8b where the PAM in the cell is oriented vertically, $F_X = -F_V cot(\theta)$, where F_H and F_V are the tensile forces produced by the horizontal and vertical PAMs calculated using Equation 2. The forces in the PAMs are a function of applied pressure and muscle contraction ratio. F_H and F_V are functions of the active lengths of the horizontal and vertical muscles, which are related to the cell angle θ by Equations 5 and 6, respectively, where $L_{fitting}$ is the length from the cell vertex to the active portion of the PAM.

$$\sigma_X = \frac{F_X}{A_X} = \frac{F_X}{2L_{link}(sin(\theta)+\alpha)\gamma L_{link}} \tag{3}$$

$$\varepsilon_X = \frac{2L_{link}(\cos(\theta)-\cos(\theta_0))}{2L_{link}(\cos(\theta_0))} = \frac{(\cos(\theta)-\cos(\theta_0))}{(\cos(\theta_0))} \tag{4}$$

$$L_H = 2L_{link}cos(\theta) - 2L_{fitting} \tag{5}$$

$$L_V = 2L_{link}sin(\theta) + \alpha L_{link} - 2L_{fitting} \tag{6}$$

$$F_X = 2F_H(\mathrm{P}, CR_H) - F_V(\mathrm{P}, CR_V)\cot(\theta) \tag{7}$$

If all three PAMs are arranged in the cell together, the total applied force in the x-direction is related to the force in the vertical and horizontal PAMs as given in Equation 7. The $2F_H$ term in Equation 7 corresponds to the tensile force applied to the vertical cell walls by the horizontal PAMs which tends to pull the vertical walls together and increase the cell angle. This change in cell shape is resisted by the vertical PAM which applies a tensile force to the top and bottom cell vertices and acts to decrease the cell angle. The tensile force applied by the vertical PAM is transferred to the horizontal direction through the inclined cell walls and corresponds to the $-F_V cot(\theta)$ term in Equation 7.

The equilibrium angle of the cell (θ_0) occurs when the magnitudes of these two opposing terms are equal and can be calculated by setting F_X to zero in Equation 7. Figure 9 illustrates the balance between these two terms for different values of pressure in the horizontal and vertical PAMs from Figures 3 and 5 (ratio of cell vertical to inclined wall length, α, is assumed to be 1). The solid experiment and dotted

simulation curves in Figure 9 labeled "Vertical PAM" are derived from the curves presented in Figure 3 but have been converted to be functions of cell angle using Equation 6, and the force values have been multiplied by $cot(\theta)$. As indicated by the left *y*-axis label, these curves represent the force applied by the vertical muscle in the horizontal direction. Similarly, the solid experiment and dashed simulation curves in Figure 9 labeled "Averaged Horizontal PAMs" are derived from the curves presented in Figure 5, but have also been converted to be functions of cell angle using Equation 5, and the force values have been scaled by a factor of 2. This set of curves, as indicated by the right *y*-axis label, represents the force applied by the horizontal muscles in the horizontal direction. For clarity, hysteresis has been removed from all the experimental curves in Figure 9 by averaging the upper and lower branches of each hysteresis loop to form a single curve.

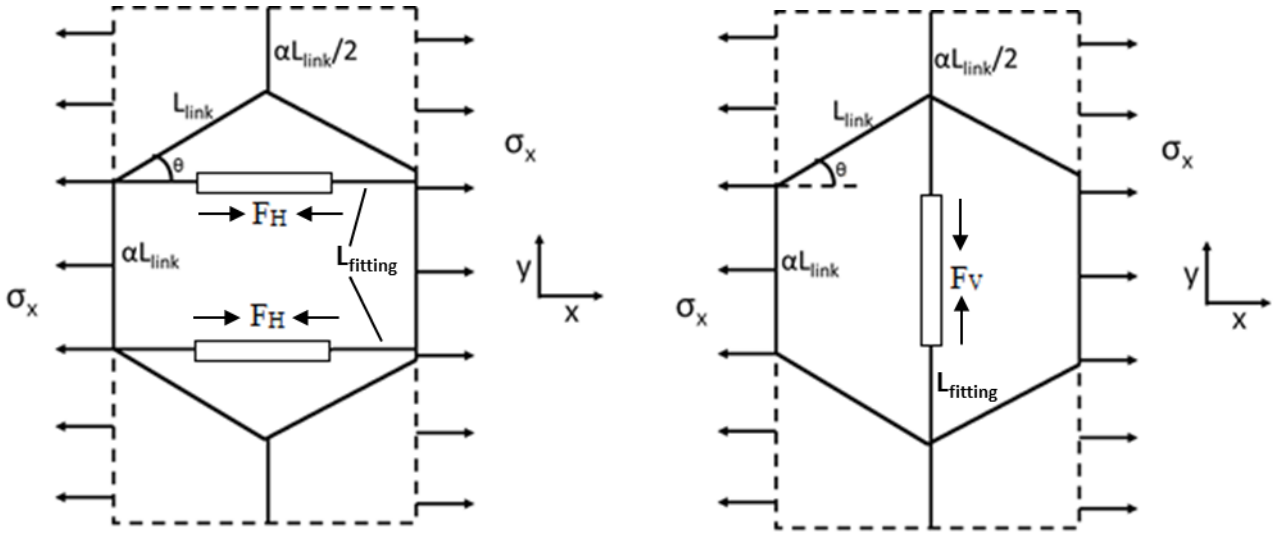

(a) (b)

Figure 8. Schematic of a pin-jointed hexagonal unit cell with (a) two horizontal PAMs and (b) a vertical PAM, with a stress applied to the cell in the horizontal direction[1].

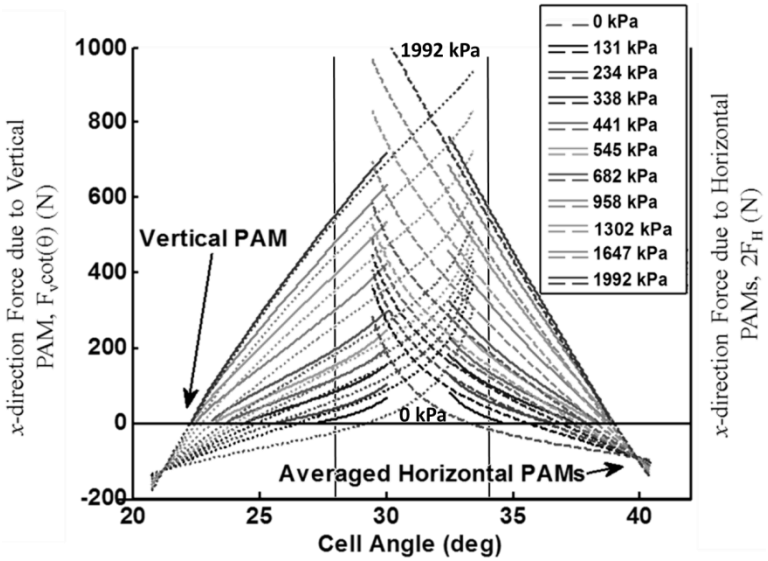

Figure 9. Tensile force versus cell angle in the horizontal direction for the vertical PAM and combined horizontal PAMs: solid curves are averaged experimental data and dashed curves are simulation.

The points in Figure 9 where the simulated curves for the vertical PAM cross those for the horizontal PAMs give the equilibrium angles for the cell (the experimental curves for individual PAMs outside the hexagonal cell were not measured to high enough contraction ratios to cross each other). From the figure it can be observed that when the vertical and horizontal PAMs are pressurized to the same level the change in cell angle is less than a degree with respect to the simulated zero-pressure equilibrium angle of 31.34°.

Even when the vertical and horizontal PAMs are pressurized to unequal pressure levels, the equilibrium cell angles remain between 28° and 34°. Consider as an example the case where the horizontal PAMs have zero pressure and the vertical PAM is pressurized to 682 kPa. The equilibrium cell angle is seen to be 29.6°. Here, the vertical PAM has contracted as a result of being pressurized from an initial contraction ratio of 106.3% to 101.4%, while the horizontal PAMs extend to a high contraction ratio of 114.1% where the tension in the muscle rises rapidly. This nonlinear stiffening in the PAM at high contraction ratios prevents significant changes in equilibrium cell angle from the zero-pressure state even when there is a large difference is pressure between the horizontal and vertical PAMs.

The slope of the force-displacement curve for the PAMs directly influences the modulus of the cell. In this study, cell modulus is calculated as a secant modulus, described by Equation 8, where the subscripts ΔF and $-\Delta F$ indicate a constant positive or negative increment in force applied to the cell about an equilibrium position (θ_0).

$$E_x = \frac{\sigma_{x\Delta F} - \sigma_{x-\Delta F}}{\varepsilon_{x\Delta F} - \varepsilon_{x-\Delta F}} = \frac{\dfrac{F_{x\Delta F}}{2\gamma {L_{link}}^2(sin(\theta_{\Delta F}) + \alpha)} - \dfrac{F_{x-\Delta F}}{2\gamma {L_{link}}^2(sin(\theta_{-\Delta F}) + \alpha)}}{\dfrac{(\cos(\theta_{\Delta F}) - \cos(\theta_0))}{(\cos(\theta_0))} - \dfrac{(\cos(\theta_{-\Delta F}) - \cos(\theta_0))}{(\cos(\theta_0))}} \tag{8}$$

Equation 8 can be simplified to illustrate that the cell modulus is dominated by the slope of the PAM force versus contraction ratio curve, and is influenced secondarily by the equilibrium cell angle. The first step in the simplification is expressed as Equation 9.

$$E_x = \frac{F_{x\Delta F}(sin(\theta_{-\Delta F}) + \alpha) - F_{x-\Delta F}(sin(\theta_{\Delta F}) + \alpha)}{(\cos(\theta_{\Delta F}) - \cos(\theta_{-\Delta F}))} \frac{\cos(\theta_0)}{2\gamma {L_{link}}^2(sin(\theta_{\Delta F}) + \alpha)(sin(\theta_{-\Delta F}) + \alpha)} \tag{9}$$

E_x can be further simplified by redefining $sin(\theta_{\Delta F})$ and $sin(\theta_{-\Delta F})$ in terms of a small increment in cell angle $\Delta\theta$ from the equilibrium position, and simplifying using the small angle assumption:

$$sin(\theta_{\Delta F}) = sin(\theta_0 - \Delta\theta) = sin(\theta_0) - \Delta\theta \cos(\theta_0) \tag{10}$$

$$sin(\theta_{-\Delta F}) = sin(\theta_0 + \Delta\theta) = sin(\theta_0) + \Delta\theta \cos(\theta_0) \tag{11}$$

Substitution of Equations 10 and 11 into Equation 9 yield

$$E_x = \frac{(F_{x\Delta F} - F_{x-\Delta F})(sin(\theta_0) + \alpha) + (F_{x\Delta F} + F_{x-\Delta F})\Delta\theta \cos(\theta_0)}{(\cos(\theta_{\Delta F}) - \cos(\theta_{-\Delta F}))} \frac{\cos(\theta_0)}{2\gamma {L_{link}}^2((sin(\theta_0) + \alpha)^2 - \Delta\theta^2 \cos^2(\theta_0))} \tag{12}$$

Recognizing that $(F_{x\Delta F} + F_{x-\Delta F}) = 0$ and that $\Delta\theta^2 \cos^2(\theta_0) \approx 0$,

$$E_x \approx \frac{(F_{x\Delta F} - F_{x-\Delta F})}{(\cos(\theta_{\Delta F}) - \cos(\theta_{-\Delta F}))} \frac{\cos(\theta_0)}{2\gamma {L_{link}}^2(sin(\theta_0) + \alpha)} \tag{13}$$

The corresponding trigonometric expressions using the small angle assumption for cosine are Equations 14 and 15.

$$cos(\theta_{\Delta F}) = cos(\theta_0 - \Delta\theta) = cos(\theta_0) + \Delta\theta \sin(\theta_0) \tag{14}$$

$$cos(\theta_{-\Delta F}) = cos(\theta_0 + \Delta\theta) = cos(\theta_0) - \Delta\theta \sin(\theta_0) \tag{15}$$

Substituting these expressions into the denominator in Equation 13, and defining $d\theta = 2\Delta\theta$, Equation 13 becomes

$$E_x \approx \frac{F_{x\Delta F} - F_{x-\Delta F}}{d\theta} \frac{\cot(\theta_0)}{2\gamma {L_{link}}^2 (sin(\theta_0) + \alpha)} \tag{16}$$

The numerator of the first term in Equation 16 is expanded by substitution of Equation 7.

$$F_{x\Delta F} - F_{x-\Delta F} = 2(F_{H\Delta F} - F_{H-\Delta F}) - \left(F_{V\Delta F} \cot(\theta_{\Delta F}) - F_{V-\Delta F} \cot(\theta_{-\Delta F})\right) \tag{17}$$

Again, Equations 10, 11, 14, and 15 are used to simplify Equation 17 and higher order terms are discarded.

$$E_x \approx \frac{2(F_{H\Delta F} - F_{H-\Delta F}) - (F_{V\Delta F} - F_{V-\Delta F}) \cot(\theta_0)}{d\theta} \frac{\cot(\theta_0)}{2\gamma {L_{link}}^2 (sin(\theta_0) + \alpha)} \tag{18}$$

The differences in the numerator of the first term are defined as $dF_H = F_{H\Delta F} - F_{H-\Delta F}$ and $dF_V = F_{V\Delta F} - F_{V-\Delta F}$. Differentiating Equations 5 and 6 and denoting the initial horizontal and vertical muscle lengths L_{H0} and L_{V0}, $d\theta$ can be expressed as:

$$d\theta = \frac{L_{H0} dCR_H}{2L_{link} cos(\theta)} = \frac{L_{V0} dCR_V}{2L_{link} cos(\theta)} \tag{19}$$

Equation 18 can thus be expressed in terms of the slope of the individual PAM force versus contraction ratios dF_H/dCR_H and dF_V/dCR_V.

$$E_x \approx \left[\frac{2}{L_{H0}} \frac{dF_H}{dCR_H} - \frac{\cot(\theta_0)}{L_{V0}} \frac{dF_V}{dCR_V}\right] \frac{cos(\theta) \cot(\theta_0)}{\gamma L_{link} (sin(\theta_0) + \alpha)} \tag{20}$$

From Figures 3 and 5 it is observed that the slopes dF_H/dCR_H and dF_V/dCR_V assume high values with increasing pressure or at very high PAM contraction ratios. Furthermore, the modulus is dependent on the interplay between the horizontal and vertical PAMs. The term outside the brackets in Equation 20 shows that the cell modulus also has a dependence on the cell geometry.

3. FABRICATION AND EXPERIMENTAL METHOD

The PAMs are fabricated by bonding 1/8" NPT steel barbed hose fittings inside both ends of a length of 6.35 mm outer diameter, 0.79 mm wall thickness latex tubing. A length of braided polyethylene terephthalate mesh sleeve, containing 120 0.19 mm diameter fibers, is then coated with epoxy at both ends and crimped over the latex tubing onto the end fittings using a 12.7 mm long, 9.34 mm inner diameter, 0.8 mm wall thickness piece of 3003 aluminum tubing.

The lengths of the muscles were designed such that for the same vertical and inclined wall lengths (α = 1) the cell would have an equilibrium angle close to 30°, while pulling the muscles into a slightly pre-tensioned state at zero pressure. This selection was made because hexagonal cellular structures with 30° cell angle and equal wall lengths are by far the most common. Measured values of the unpressurized active lengths of the muscles, L_0, are given in Table 1. When assembled in the cell under no load, the vertical muscle was at a measured contraction ratio of 106.3%, and the two horizontal muscles were at a contraction ratio of 107.6%, giving the unit cell a measured equilibrium angle of 31.34°.

The hexagonal cell itself is fabricated from dogbone-shaped aluminum links pinned together at their endpoints. Each link contains a ball bearing at both ends to decrease friction and further reduce contributions from sources other than the PAM stiffness to the modulus of the cell. Each wall of the hexagonal cell contains two links stacked in an order that allows the cell to be expanded to a multi-cell array if desired. The vertical walls of the cell also contain a third triangular-shaped link with a tab that can be gripped by an Instron machine for experimental testing, as seen in Figure 1. PAMs are connected between the vertices of the cell and supplied with air pressure by modified brass pressure fittings. The length from the pin to the active portion of each muscle ($L_{fitting}$) is listed in Table 2 along with the other cell parameters.

Table 2. Hexagonal unit cell parameters

L_{link} (m)	0.1111
$L_{fitting}$ Horizontal (m)	0.0676
$L_{fitting}$ Vertical (m)	0.0650
α	1
γ	0.4140

Figure 10 shows a photograph of the hexagonal cell with all three PAM inclusions fixed in an Instron model 4204 machine with a 5 kN load transducer. The cell is oriented such that the grips of the machine are holding the vertical walls of the cell to load it in the *x*-direction. Three sets of experiments were performed pressurizing only the two horizontal PAMs, only the vertical PAM, and pressurizing all three PAMs simultaneously. The PAMs were supplied industrial air from a 49L cylinder, pressurized to 17,237 kPa, and regulated by a Harris model 721 pressure regulator. Pressure was measured after the regulator but before the PAMs using an Omega PX4100-1KGV pressure transducer and a National Instruments USB-6212 data acquisition system. At each pressure, the Instron machine pulled the cell in tension to a load of 200 N at a rate of 10 N/s, then reversed direction and applied a compressive load to -100 N, and finally returned to the initial equilibrium position of the cell. The maximum pressure for the experiments with all three PAMs in the cell was limited to 682 kPa to avoid PAM failure, but this limit was likely overly cautious as the individual PAMs performed at 1992 kPa without failure. Thus, high pressure simulation of the hexagonal cell presented in the following sections is plausible.

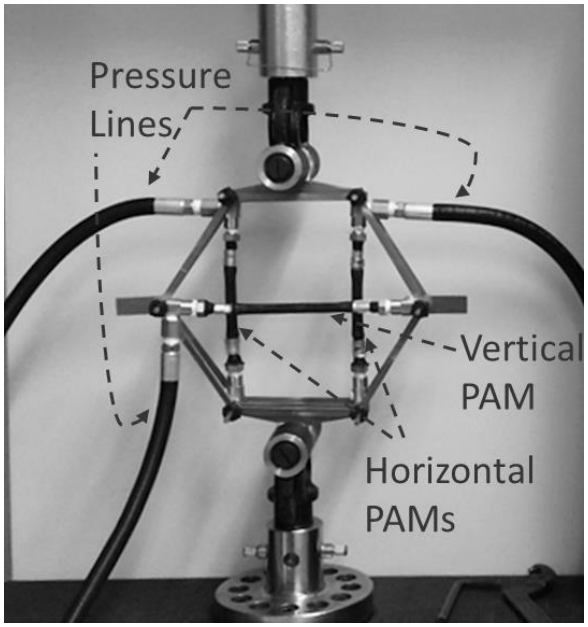

Figure 10. Hexagonal cell with three PAM inclusions fixed in the Instron machine for loading in the horizontal direction.

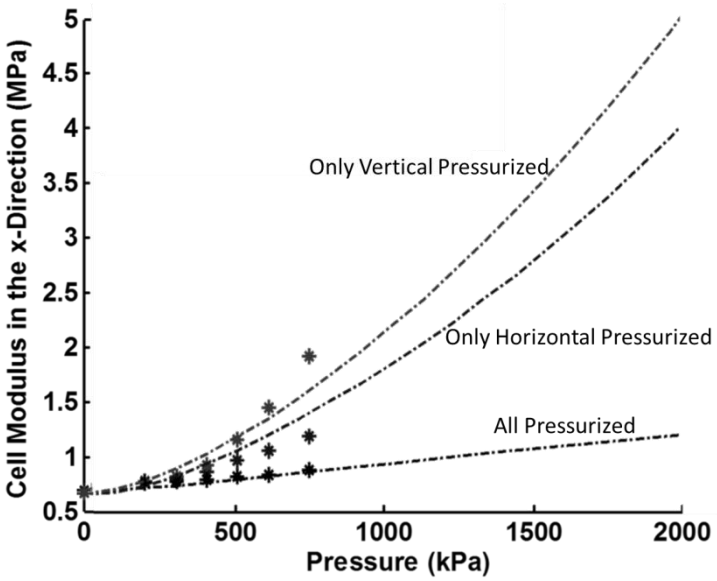

Figure 11. Cell modulus in the horizontal direction as a function of pressure.

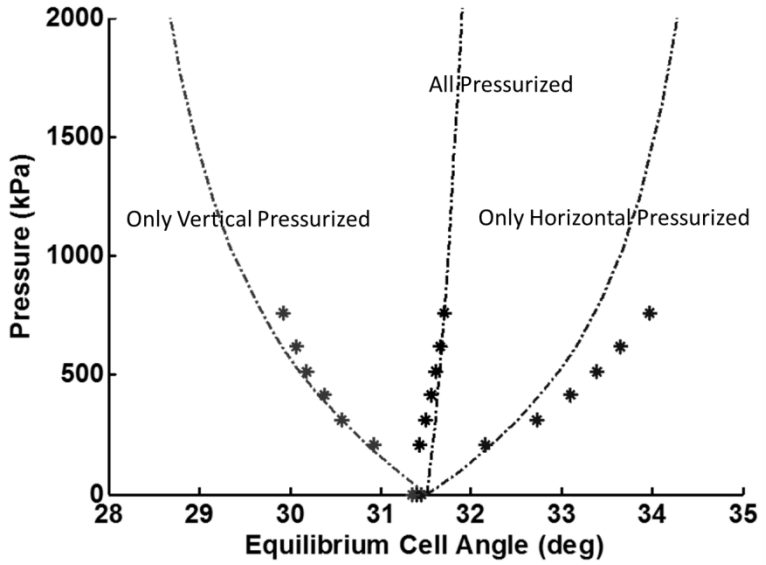

Figure 12. Equilibrium cell angle.

4. RESULTS

Figure 11 shows the variation in the hexagonal cell modulus in the horizontal (*x*) direction with increasing pressure, where the data points are the measured values from experiment and the dashed curves represent the simulation results. There is good agreement between the experiment and simulation when all three PAMs are pressurized together, but the simulation overpredicts modulus by a maximum of 15% at 682 kPa when only the horizontal PAMs are pressurized, and underpredicts modulus by 10% at 682 kPa when only the vertical PAMs are pressurized. As discussed in Section 2.2, the hexagonal cell's initial geometry balances the forces generated by the vertical and horizontal PAMs. Therefore, increasing the pressure in all three PAMs equally is not an effective approach to increasing the modulus of the cell. The data shows that even when all three PAMs are pressurized to 1992 kPa, the increase in modulus is only

80%. Instead, the PAMs must be pressurized differentially to realize larger changes in modulus. The greatest change in modulus is achieved by pressurizing only the vertical PAM. Experimentally, an increase in modulus from 0.65 MPa to 1.95 MPa (a 200% increase) was measured at 682 kPa, and simulation indicates that at 1992 kPa the modulus would increase to 4.98 MPa (a 666% increase). The corresponding change in cell angle is 1.53^{o} for the experimental measurement at 682 kPa, and 2.75^{o} for the simulation at 1992 kPa, as shown in Figure 12.

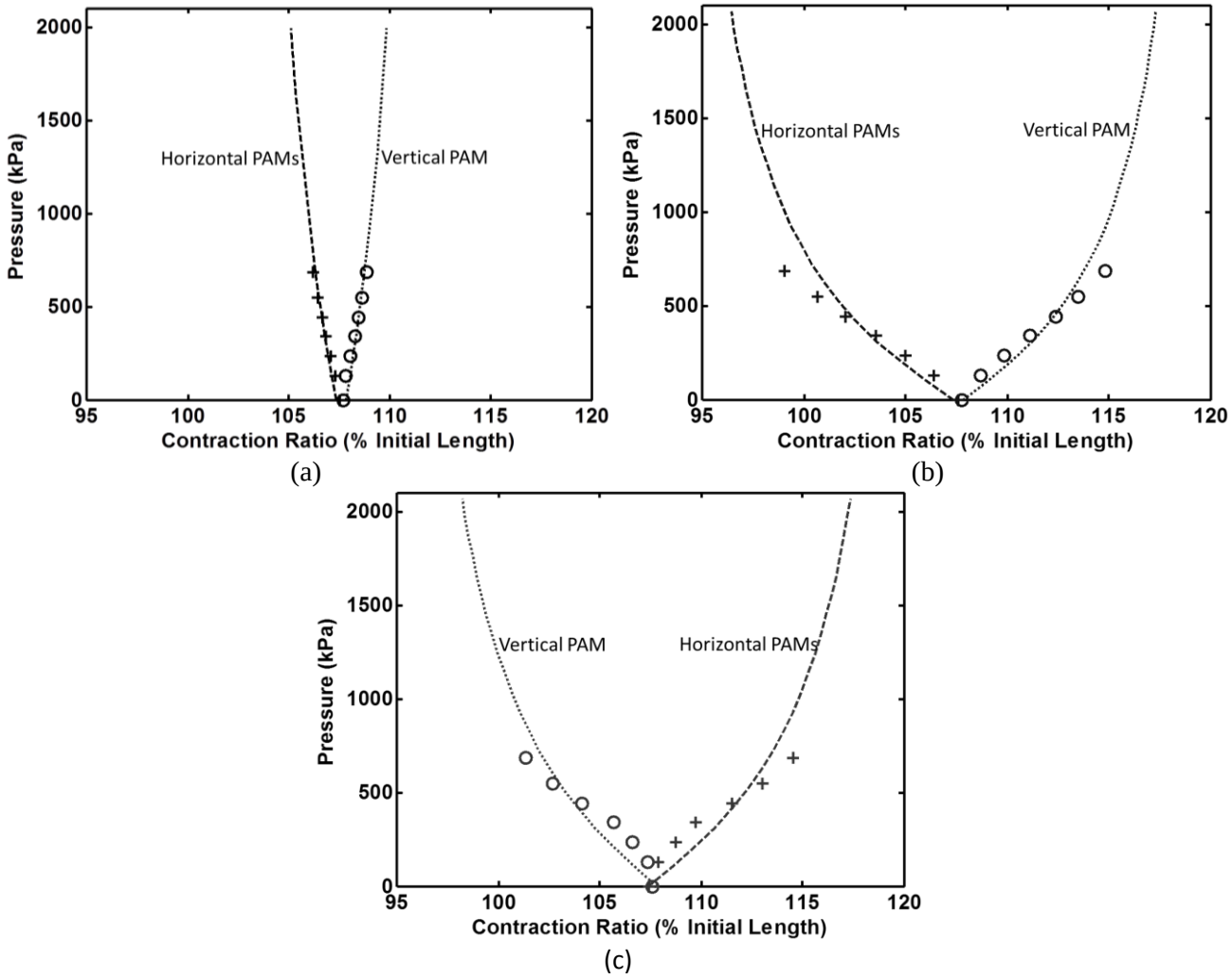

Figure 13. Equilibrium contraction ratio as a function of pressure when (a) all three PAMs are pressurized (b) only the horizontal PAMs are pressurized and (c) only the vertical PAM is pressurized.

Figure 13 shows a comparison of experimental measurements (symbols) and model predictions (dashed or dotted lines) for contraction ratios in the horizontal and vertical PAMs with increasing pressure. Recall from the discussion of Equation 20 that the modulus of the cell is determined by the slope of the individual PAM force versus contraction ratio curves. The highest slopes in Figure 3 and Figure 5 occur where the PAMs are unpressurized but at very high contraction ratios. Thus, the large increase in E_x seen in Figure 11 by pressurizing the vertical PAM is achieved because this stretches the horizontal PAMs to very high contraction ratios. This reasoning is confirmed by Figure 13c, which shows that the highest contraction ratios occur in the horizontal PAMs when the vertical PAM is pressurized. This maximum modulus configuration depends heavily on the relative values of the muscle parameters, especially the initial contraction ratio of the muscles.

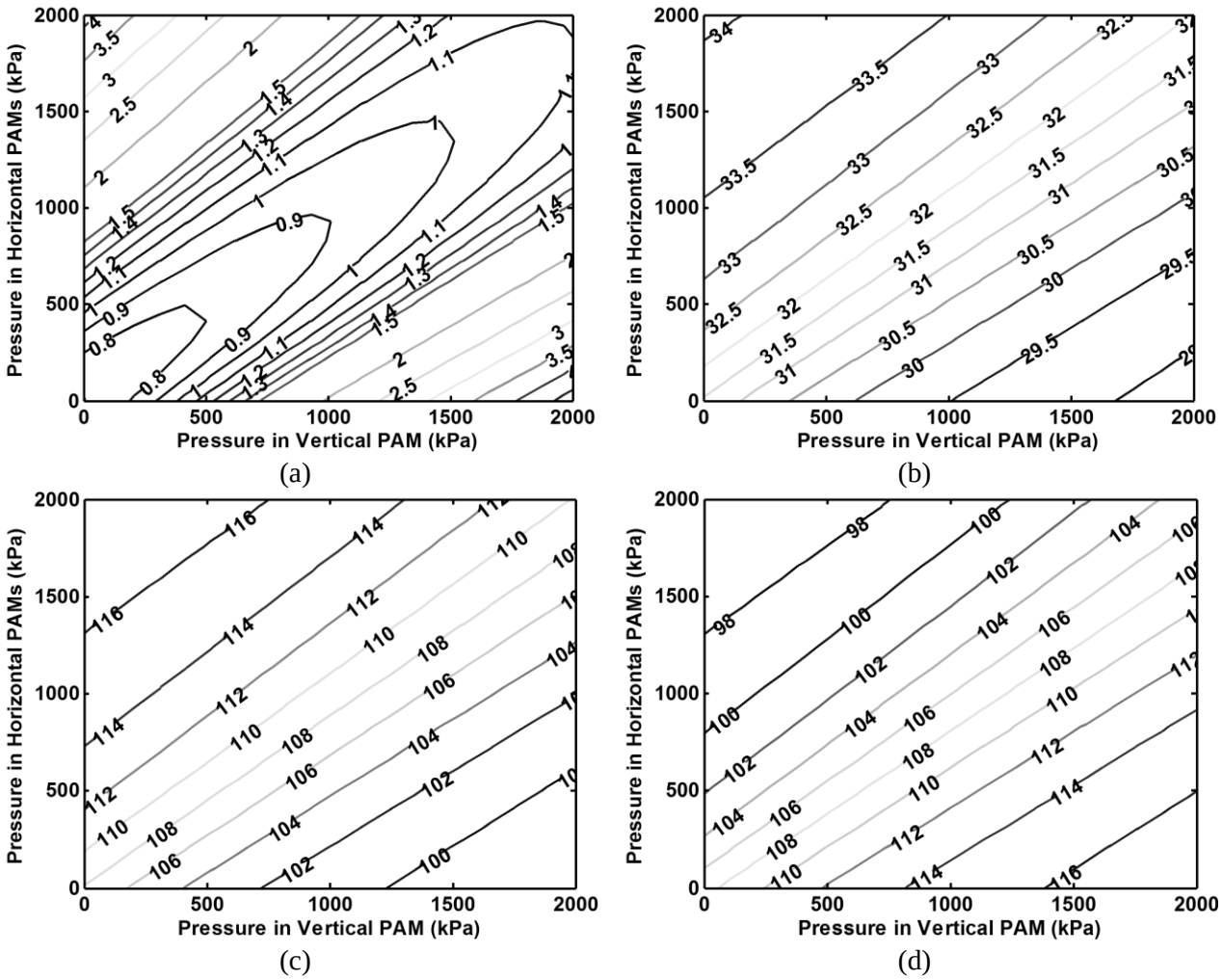

Figure 14. Simulated (a) Cell modulus in the horizontal direction in MPa (b) Equilibrium cell angle in degrees (c) Vertical PAM contraction ratio and (d) Horizontal PAM contraction ratio calculated over a range of differential pressures in the PAMs.

Another point of note is that the simulation in Figure 13a captures the trend that as pressure is increased equally in all three PAMs, the horizontal PAMs produce slightly more force than the vertical PAM, causing the contraction ratio of the horizontal PAMs to decrease, the contraction ratio of the vertical PAM to increase, and the overall cell angle to increase slightly (Figure 12). Although the trends are captured by the simulation, in all pressurization cases there seems to be a vertical offset of approximately 250 kPa in the experiment compared with simulation. This may represent that the physical PAMs required some initial pressure to begin contracting.

Consider Figure 14a, where the pressures in the vertical and horizontal PAMs vary independently from 0 to 1992 kPa and the values of the contours are the cell modulus E_x in MPa. In the simulation and experiments discussed above, only data points along each of the Figure 14a axes and the $y=x$ line were investigated. Figure 14a uses the simulation to fill in the operational space. As expected, the highest values of cell modulus fall far from the $y=x$ line in the upper left and lower right corners of the plot where either the horizontal or the vertical PAMs are completely unpressurized, while the other is fully pressurized. The corresponding cell angles and contraction ratios in the horizontal and vertical muscles are plotted in Figure 14b-d, respectively. In Figure 14b, pressurizing the vertical PAM is seen to decrease the cell angle while pressurizing the horizontal PAMs does the reverse. In Figures 14c and 14d, notice that the contraction ratios for a given muscle are never below 97% when the muscle is unpressurized, which means that the

muscles barely ever enter compression in the design space. In Figure 14c, moving along the *x*-axis, pressurizing the vertical PAM reduces its contraction ratio, but simultaneously pressurizing the horizontal PAM resists this contraction. In fact, high pressure in the horizontal PAMs with low-to-moderate pressure in the vertical PAM will force the vertical PAM to stretch. Similarly, in Figure 14d, moving up the *y*-axis, pressurizing the horizontal PAMs reduces their contraction ratios but simultaneously pressurizing the vertical PAMs resists this contraction. High pressure in the vertical PAMs with low-to-moderate pressure in the horizontal PAMs will force the horizontal PAMs to stretch. Figure 14a shows a maximum change in cell modulus (ΔE_x) of 666% when the vertical PAM is pressurized to 1992 kPa and the horizontal PAM is left unpressurized. The cell angle reduces to 28.59^o from a zero-pressure equilibrium cell angle of 31.34^o. The pressurized vertical PAM contraction ratio is 98.18% (down from a zero pressure contraction ratio of 106.3%) and the unpressured horizontal PAM contraction ratio increases to 117.4% (up from a pressure of 107.6% when no pressure was in the vertical PAMs).

5. DESIGN STUDY

In the previous section, the vertical and inclined walls of the cell had the same length (α=1), and the zero pressure equilibrium cell angle was held close to 30^o. This section examines whether greater changes in modulus may be realized by pressurizing the PAMs in different cell geometries. The vertical to inclined wall length ratio is varied between α=0.5 to 2, and the zero pressure equilibrium cell angle is varied from θ=10^o to 50^o. Further, for any given cell geometry, the PAM contraction ratios are varied as well. Four different values, a minimum of 100%, intermediate values of 104% and 107.6%, and a maximum value of 108.3% are used for the vertical PAM. In comparison, the previous section considered only single values of 106.3% and 107.6% for the vertical and horizontal PAM contraction ratios, respectively.

Figure 15 provides a flow chart of the process used to determine the maximum ΔE_x achievable. For a selected value of cell geometry parameters, α and θ, the four different values of vertical PAM contraction ratio are considered. For each value, the horizontal PAM contraction ratio required for the cell to maintain the selected zero pressure equilibrium angle, θ_o, is calculated. This step assumes that the PAMs have the same initial fiber angles, unpressurized wall thickness, unpressurized radius, and bladder modulus used for simulation of the prototype (Table 1), but the active length changes based on the cell geometry. For a vertical PAM contraction ratio of 100%, the horizontal PAMs are at 100% contraction ratio, as well. But for vertical PAM contraction ratios greater than 100%, the horizontal PAMs need to be pre-stretched as well to balance the forces exerted on the cell by the vertical PAM, and to hold the cell in equilibrium at the desired angle. Figure 16 shows the horizontal PAM contraction ratio versus equilibrium cell angle for increasing values of vertical PAM contraction ratio (marked on the curves). For vertical PAM contraction ratios greater than 100%, the horizontal PAM contraction ratios are equal for cell angles ranging from 30.59^o to 31.58^o. For higher cell angles (steeper cells), the horizontal PAM contraction ratios are lower, while for lower cell angles (shallower cells), the horizontal PAMs are stretched to higher contraction ratios. Note that the results in Figure 16 are independent of α because force produced by a given muscle (which determines equilibrium angle) is dependent only on the contraction ratio, not the physical length of the muscle.

For the current values of cell geometric parameters and PAM contraction ratios, the unstretched length of the vertical and horizontal PAMs is calculated assuming the prototype values of $L_{fitting}$ and L_{link}. Provided the calculated PAM lengths are greater than a minimum threshold value, the cell modulus in the *x*-direction is calculated for the zero pressure and three maximum pressurization cases as described in Section 4 and listed in the 6th step of Figure 15. For the maximum pressure cases a check was instituted to ensure that none of the PAMs within the cell were stretched beyond their physical limit. Equation 21, derived from Equation 1, describes the relationship between contraction ratio of the PAM and the bladder wall thickness.

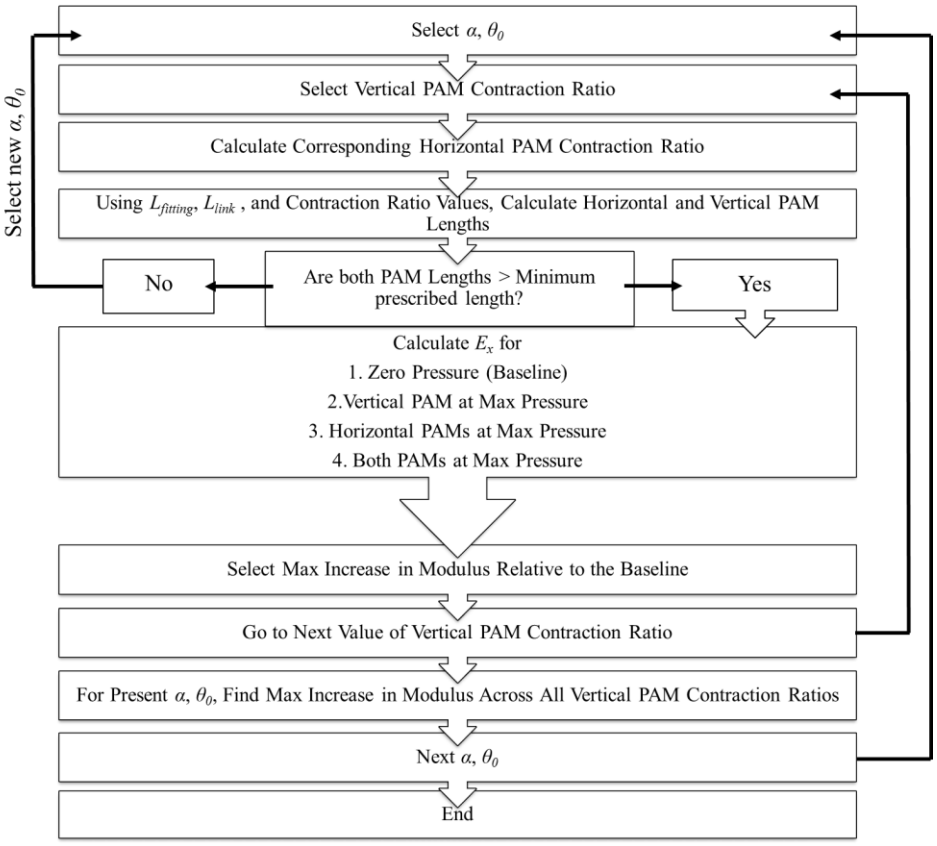

Figure 15. Flow chart of the process used to determine the maximum achievable *x*-direction change in cell modulus over a range of contraction ratios, cell angles, and wall length ratios.

$$t = R - \sqrt{R^2 - \frac{1}{CR}\left({R_0}^2 - (R_0 - t_0)^2\right)} \tag{21}$$

In order for *t* to be real, the quantity under the square root in Equation 21, which depends on contraction ratio, must be greater than zero. This limits the maximum contraction ratio of the vertical muscle to 118.05% and the maximum contraction ratio of the horizontal muscles to 119.68%. If in any of the pressurized equilibrium states of the cell the muscles exceed these limits, that case is eliminated from consideration.

For the feasible cases, the maximum change in cell modulus between the zero pressure state and one of the pressurized states is recorded, and the process is repeated for the next vertical muscle contraction ratio. After all contraction ratios are evaluated, the overall greatest change in cell modulus is determined for that point in the design space. The results of this design study are presented in Figure 17, where the labeled contours represent the maximum percent change in cell modulus relative to the zero pressure case. The gray shaded region in Figure 17 represents areas where maximum change in modulus is realized by pressurizing only the horizontal PAMs. Elsewhere, the maximum change is realized by pressuring only the vertical PAMs. The blacked out region at the extreme bottom left represents an infeasible area of the design space where the vertical PAM length is below a minimum threshold.

Figures 18a and 18b consider a couple of design points in greater detail. For α=1 and θ_0=20.5^o, (in the grey region in Figure 17), Figure 18a plots the cell modulus as a function of pressure. Clearly, the increase in modulus is greater when the horizontal PAMs are pressurized. In comparison, Figure 18b for α=1 and θ_0=41.5^o (in the unshaded region in Figure 17) shows the greatest increase in modulus is achieved by pressuring only the vertical PAM. Another point to note is that although the percent change in modulus for the case in Figure 18b is larger than that in Figure 18a, the magnitude of the maximum modulus in

Figure 18a is over 2.5 times larger than that in Figure 18b. Evidently, the low zero pressure modulus is a strong contributor to a high change in modulus in Figure 18b.

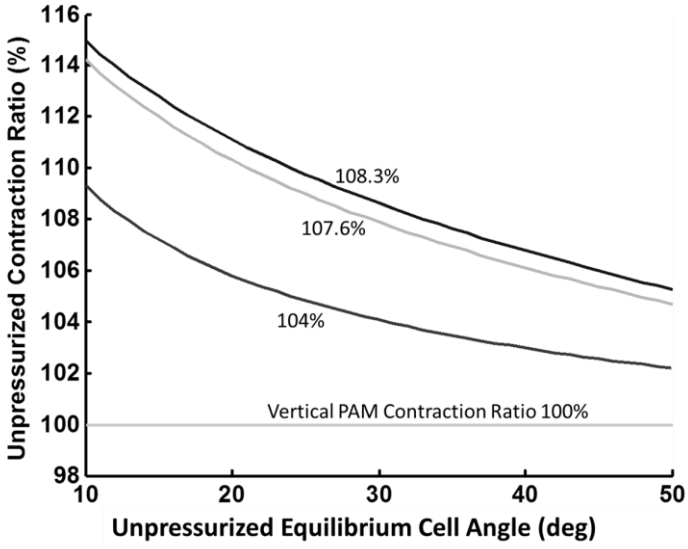

Figure 16. Unpressurized horizontal PAM contraction ratios corresponding to the labeled prescribed values of vertical PAM contraction ratio for a range of equilibrium cell angles.

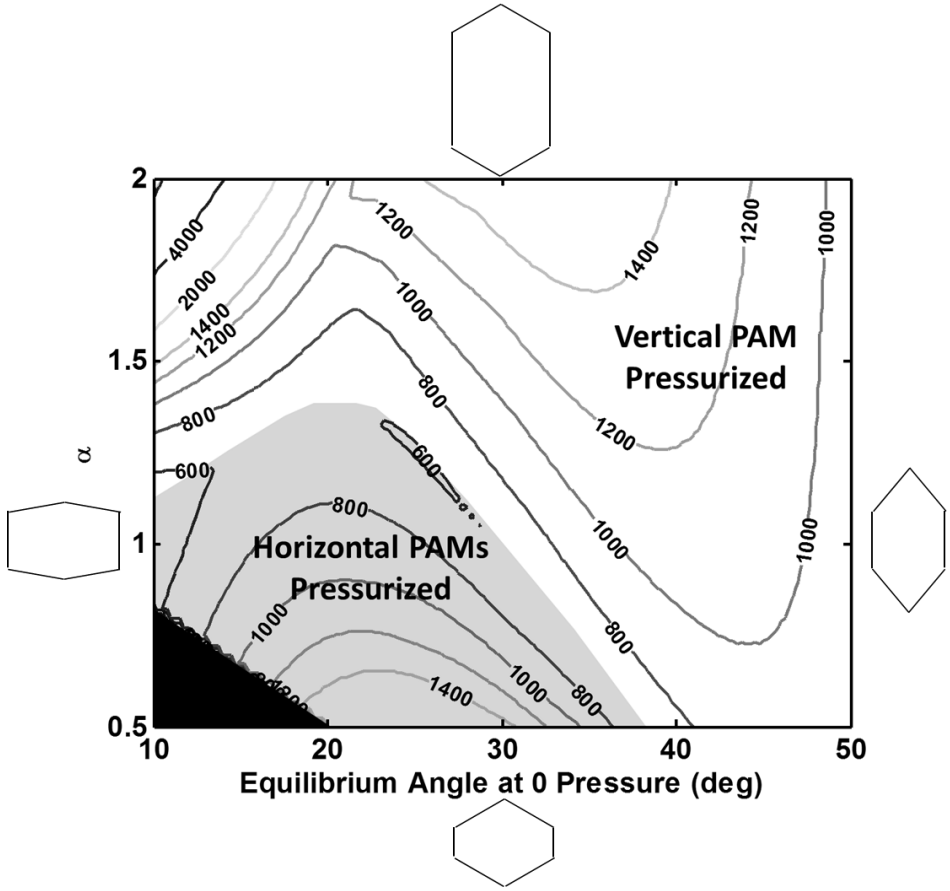

Figure 17. Maximum change in cell modulus (%) as a function of vertical wall length ratio (α) and equilibrium cell angle.

Figure 19a presents the zero pressure modulus with reference to which the maximum increase in modulus in Figure 17 is calculated, and Figure 19b shows the corresponding change in cell angle due to pressurization. These two plots, combined with Figure 17, serve as useful guides for selecting the best cell geometry in the design space that maximizes ΔE_x, while considering other constraints. There are three regions in Figure 17 where ΔE_x exceeds 1400%: the top left region, the top middle region, and the bottom left/middle region. Of those regions, Figure 19b shows that the top left of the plot has the highest changes in cell angle (exceeding 10^o), which is generally undesirable unless active shape change is a design goal. Therefore, the bottom left/middle region and the top middle region are more ideal for generating large changes in cell modulus for low changes in cell angle. Figure 19a shows that of these two regions, the top middle has a lower zero pressure cell modulus of less than 0.2 MPa and therefore also a lower pressurized cell modulus. Thus, the region that achieves the highest absolute cell modulus while also allowing for large ΔE_x and low changes in cell angle is the region below α=0.7 between zero pressure equilibrium cell angles of 20^o and 30^o. The maximum modulus in this region of 414 MPa is achieved at α=0.5 and θ_0=20^o, where the cross-sectional area of the cell in the *x*-direction is at the minimum possible value and the horizontal PAMs are fully pressurized to resist loading in the *x*-direction. In this region, however, the length of the vertical PAM is very short. A more reasonable design point with a feasible muscle length in the same region is α=0.7 and θ_0=25^o. The system parameters associated with this design point are listed in Table 3.

The reason for the distinct regions evident in Figure 19 is the discrete choices for starting vertical PAM contraction ratio used in the iterative loop of the design study. Figure 20a shows the initial contraction ratio of the vertical PAM corresponding to the results presented in Figures 17 and 19. Recall that within the loop, a check was made to eliminate any cell configurations where the pressurization of the PAMs caused the contraction ratio of the orthogonal PAMs to exceed the maximum limit. At high starting contraction ratios of the vertical PAM, all the PAMs within the cell were pre-strained before pressurization and therefore exceeded the contraction ratio limit when pressurized more easily. When this limit was exceeded, the pressurization case was eliminated from consideration. Therefore, the majority of maximum ΔE_x cases occurred at low starting vertical PAM contraction ratios (100% and 104%) because the higher starting contraction ratio cases (107.6% and 108.3%) had exceeded the limits of the muscles.

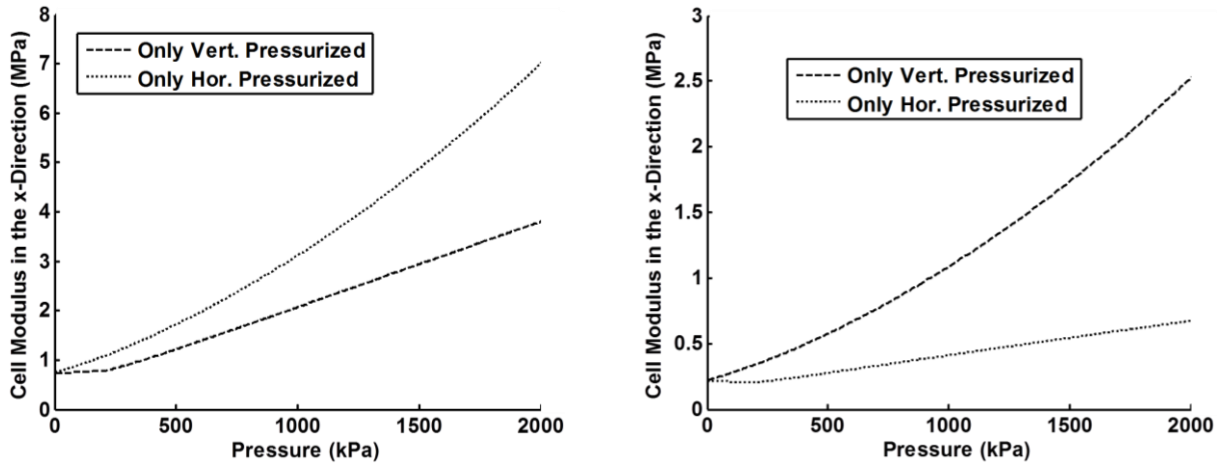

Figure 18. Cell modulus as a function of pressure for (a) α=1 and θ_0=20.5 and (b) α=1 and θ_0=41.5.

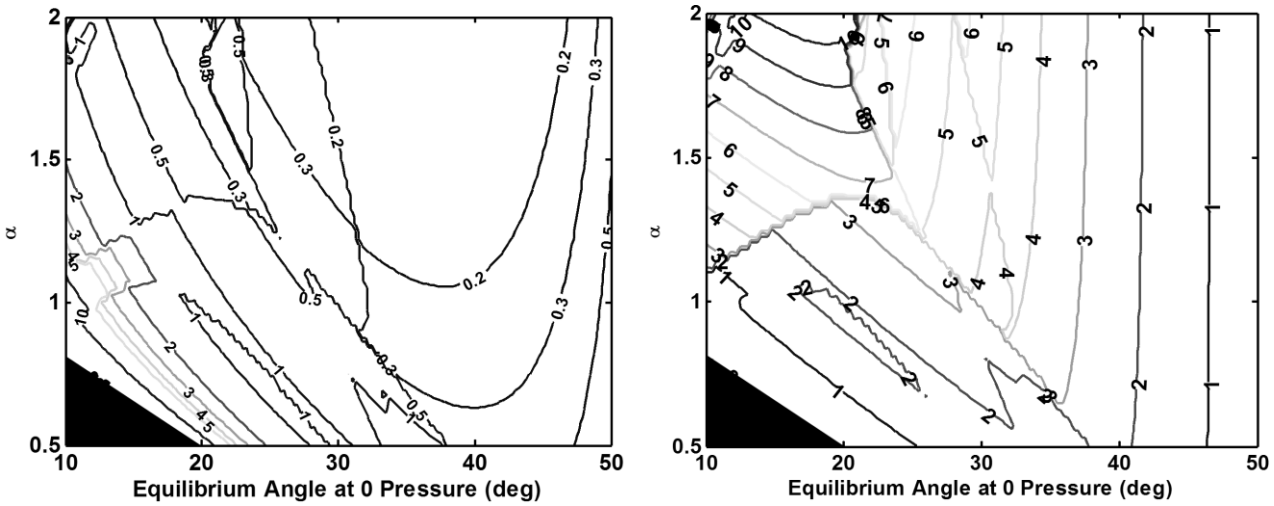

(a) (b)

Figure 19. (a) Zero pressure cell modulus corresponding to the maximum change in cell modulus (MPa) and (b) change in cell angle corresponding to maximum change in cell modulus (deg).

Table 3. System parameters at the design point where α=0.7 and θ_0=25°.

PAM Parameters	
L_H	66.2 mm
L_V	42.7 mm
Horizontal θ_{b0}	52.39°
Vertical θ_{b0}	53.58°
t_0	0.8 mm
R_0	4.8 mm
E	3 MPa
Cell Parameters	
L_{link}	111.1 mm
L_{Hfit}	67.6 mm
L_{Vfit}	64.5 mm
α	0.7
γ	0.4140
θ_0	25°
Resulting System Parameters	
Horizontal PAMs Eq. CR	100%
Vertical PAM Eq. CR	100%
Modulus, 0 kPa	0.81 MPa
Max. Modulus, 1992 kPa (Only Horizontal PAMs Pressurized)	11.00 MPa
Change in Cell Angle	1.96°
Max. Change in Modulus	1258%

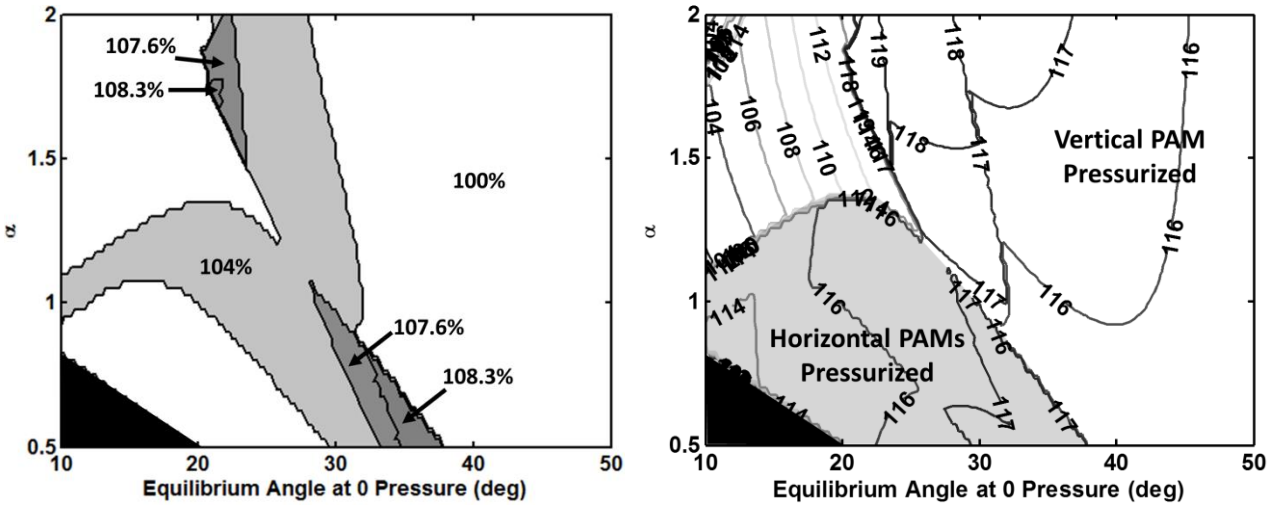

(a) (b)

Figure 20. (a) Unpressurized equilibrium contraction ratio of the vertical PAM corresponding to the maximum change in cell modulus and (b) maximum pressurized equilibrium contraction ratio (%) of any PAM within the cell.

Figure 20b plots the maximum contraction ratio of any PAM within the cell in the pressurized equilibrium state corresponding to the maximum ΔE_x. This figure shows that at the borders of the regions in Figure 20a, the contraction ratio of the PAMs have been pushed to the limit. At the borders of the gray region in Figure 20b, which corresponds to the region where the horizontal PAMs are pressurized to achieve a maximum ΔE_x, the maximum contraction ratio in the vertical PAM does not exceed the 118% limit. In the region where the vertical PAMs are fully pressurized, maximum ΔE_x is achieved by pre-straining the horizontal PAMs as much as possible. Again, at the borders where the zero-pressure vertical PAM contraction ratio changes in Figure 20a, the maximum horizontal PAM contraction ratio has been pushed nearly to its limit of 119.68%. If the parametric study for maximum ΔE_x were performed using smaller increments in vertical PAM contraction ratio values, every value in Figure 20b would be nearly equal to either the horizontal or the vertical PAM contraction ratio limit.

6. SUMMARY AND CONCLUSIONS

This work has presented a novel variable modulus cellular structure comprised of hexagonal unit cells with PAM inclusions. The cell considered is a pin-jointed hexagonal unit cell, loaded in the horizontal direction, with three PAMs oriented in an "H" pattern between the vertices of the cell: one vertical PAM and two horizontal PAMs. A model of the PAMs assuming a constant volume of bladder material was shown to compare well with force-displacement measurements of the individual PAMs used within the cell. A method for calculation of the hexagonal cell modulus based on an approach used for linear springs within the cell was introduced, as was an expression for the balance of tensile forces between the horizontal and vertical PAMs.

An aluminum hexagonal unit cell was fabricated and simulation of the hexagonal cell with PAM inclusions was then compared to experimental measurement of the unit cell modulus in the horizontal direction with the PAMs pressurized over a pressure range up to 682 kPa. An increase in cell modulus by a factor of 2 and a corresponding change in cell angle of only 1.53^o were demonstrated experimentally. A design study via simulation predicts that differential pressurization of the PAMs up to 1992 kPa can increase the cell modulus in the horizontal direction by a factor of 6.66 with a change in cell angle of only 2.75^o, and that by varying the cell geometry changes in modulus greater than 1000% are possible while

maintaining changes in cell angle below 3^o. The experiment and simulation show that this concept provides a way to largely decouple the length change of a PAM from the change in modulus to create a structural unit cell whose in-plane modulus in a given direction can be tuned based on the orientation of PAMs within the cell and the pressure supplied to the individual muscles.

ACKNOWLEDGMENTS

The authors acknowledge funding of these research activities by Dr. David Stargel through the Air Force Office of Scientific Research (grant numbers FA9550-11-1-0159 and 4767-RPI-AFOSR-0159).

REFERENCES

1. Pontecorvo, M.E., Barbarino, S., and Gandhi, F.S., "Cellular honeycomb-like structures with internal inclusions in the unit-cell," Proceedings of the ASME 2012 Conference on Smart Materials, Adaptive Structures and Intelligent Systems, Stone Mountain, Georgia, USA, September 19-21, (2012).
2. Barbarino, S., Pontecorvo, M.E., and Gandhi, F.S., "Cellular honeycomb-like structures with internal buckling and viscous elements for simultaneous load-bearing and dissipative capability," Proceedings of the ASME 2012 Conference on Smart Materials, Adaptive Structures and Intelligent Systems, Stone Mountain, Georgia, USA, September 19-21, (2012).
3. Bland, S.M., Snyder, R.J., Kudva, J.N., Barbarino, S., Pontecorvo, M.E., Gandhi, F.S., and White, E.V., "A novel structural element combining load carrying and energy dissipation capability", Proceedings of the AIAA SciTech 2014 Conference, National Harbor, Maryland, USA, January 13-17, (2014).
4. Gaylord, R., *Fluid actuated motor system and stroking device*, U.S. Patent No. 2,844,126, (1958).
5. Schulte, H., "The characteristics of the McKibben artificial muscle," The Application of External Power in Prosthetics and Orthotics, Publication 874, National Academy of Sciences - National Research Council, Washington DC, Appendix H, pp. 94-115, (1961).
6. Philen, M., "Fluidic flexible matric composite semi-active vibration isolation mounts," Journal of Intelligent Material Systems and Structures, 23, 353-363 (2012).
7. Philen, M., "Force tracking control of fluidic flexible matrix composite variable stiffness structures," Journal of Intelligent Material Systems and Structures, 22, 31-43 (2011).
8. Philen, M., "Tunable modulus structures utilizing fluidic flexible matrix composites: analytical and experimental investigations," 51st AIAA/ASME/ASCE/AHS/ASC Structures, Structural Dynamics, and Materials Conference, (2010).
9. Philen, M., "Sliding mode control of variable modulus structures based upon fluidic flexible matrix composites," 49th AIAA/ASME/ASCE/AHS/ASC Structures, Structural Dynamics, and Materials Conference, (2008).
10. Philen, M., "On the applicability of fluidic flexible matrix composite variable impedance materials for prosthetic and orthotic devices," Smart Materials and Structures, 18 (2009).
11. Chen, Y., Yin, W., Liu, Y. & Leng, J., "Structural design and analysis of morphing skin embedded with pneumatic muscle fibers," Smart Materials and Structures, 20 (2011).
12. Kim, G.-W., Li, S. & Wang, K., Ghasemi-Nejhad, M. N. (Ed.), "Variable stiffness actuator based on fluidic flexible matrix composites and piezoelectric-hydraulic pump," Active and Passive Smart Structures and Integrated Systems, 7643 (2010).
13. Kothera, C. S., Jangid, M., Sirohi, J. & Wereley, N. M., "Experimental characterization and static modeling of McKibben Actuators," *Journal of Mechanical Design,* (2009).